nature materials

ARTICLES

PUBLISHED ONLINE: 11 JANUARY 2016 | DOI: 10.1038/NMAT4536

Defined three-dimensional microenvironments boost induction of pluripotency

Massimiliano Caiazzo[1†], Yuya Okawa[1†], Adrian Ranga[1], Alessandra Piersigilli[2], Yoji Tabata[1] and Matthias P. Lutolf[1,3*]

Since the discovery of induced pluripotent stem cells (iPSCs), numerous approaches have been explored to improve the original protocol, which is based on a two-dimensional (2D) cell-culture system. Surprisingly, nothing is known about the effect of a more biologically faithful 3D environment on somatic-cell reprogramming. Here, we report a systematic analysis of how reprogramming of somatic cells occurs within engineered 3D extracellular matrices. By modulating microenvironmental stiffness, degradability and biochemical composition, we have identified a previously unknown role for biophysical effectors in the promotion of iPSC generation. We find that the physical cell confinement imposed by the 3D microenvironment boosts reprogramming through an accelerated mesenchymal-to-epithelial transition and increased epigenetic remodelling. We conclude that 3D microenvironmental signals act synergistically with reprogramming transcription factors to increase somatic plasticity.

The manipulation of mammalian cell morphology can induce a variety of behavioural changes including proliferation, migration, apoptosis and differentiation[1–7]. These morphologically driven processes are directly controlled by the cell microenvironment, and there is mounting evidence that biophysical signals conveyed by the extracellular matrix (ECM) are responsible for these changes in cell fate[8–10]. On a molecular level, shape-induced cell fate changes are controlled by changes in gene expression patterns, which themselves are precisely regulated by chromatin organization through a number of different post-translational histone modifications such as acetylation and methylation[11].

Reprogramming of somatic cells is considered to be a multi-step process characterized by an early and late phase of transcriptome and proteome resetting[12]. Notably, genome-wide analysis has revealed that intermediate cell populations that eventually form iPSCs are characterized by the activation of genes responsible for cytoskeleton organization during the first three days of reprogramming[13], and quantitative proteomic analysis has shown strong induction of proteins related to the regulation of chromatin organization during the same time frame[14]. Taken together, cytoskeletal and epigenetic alterations are two critical events that mark the initiation phase of the reprogramming process.

Although previous studies have demonstrated profound effects of the ECM on cell shape and accompanying alteration in chromatin structure, and recent work has revealed that iPSC generation can be influenced by biophysical parameters in 2D culture[15], the role of 3D microenvironmental cues on somatic-cell reprogramming remains unexplored. To characterize these essential early events in establishing the pluripotent state of iPSCs, we report a new reprogramming strategy using chemically defined 3D ECMs (ref. 5). Such matrices permit a precise control over the physiochemical characteristics of the cellular microenvironment that is unachievable in 2D culture systems. We demonstrate that biophysical effectors linked to 3D cell confinement induce immediate alterations in cell morphology that facilitate mesenchymal-to-epithelial transition (MET), as well as histone modifications essential for the initiation of reprogramming. These results suggest previously unknown mechanisms underlying somatic-cell reprogramming and highlight the functional importance of the interaction between cells and their ECM in the regulation of cell fate.

3D microenvironments to promote pluripotency

To find an optimal synthetic microenvironment for iPSC generation, we first used mouse embryonic stem cells (ESCs) to determine 3D matrix compositions that best promote ESC self-renewal and pluripotency. To do so, we modulated the mechanical properties of enzymatically crosslinked poly(ethylene glycol) (PEG)-based hydrogels by varying polymer content[16,17]. Additionally, to mimic the biochemical features of native ECMs, we functionalized the otherwise inert PEG network with the fibronectin-derived adhesion peptide RGDSP (arginine-glycine-aspartate-serine-proline). We then encapsulated ESCs in soft gels (shear modulus $G' = 300 \pm 35$ Pa, as determined by rheometry) using either matrix metalloproteinase (MMP)-degradable (containing the MMP substrate GPQG↓IWGQ; ↓ indicating the cleavage site) or -nondegradable (containing the MMP-insensitive sequence GDQGIAGF) PEG networks[18]. The results clearly showed that degradable gels allowed for better cell proliferation (Supplementary Fig. 1a–c). We further quantified ESC proliferation in gels of variable stiffness and cell seeding density (Supplementary Fig. 1d–h). These experiments, consistent with our recently published data[19], showed that degradable and soft gels, at a seeding density of 1,000 cells μl^{-1}, resulted in optimal proliferation rates similar to the 2D control condition, and gave rise to the highest levels of pluripotency marker expression (Supplementary Fig. 1i). Indeed, following encapsulation in 3D gels, individual ESCs were uniformly distributed throughout these matrices and expanded into colonies of cells positive for NANOG, OCT4

[1]Laboratory of Stem Cell Bioengineering, Institute of Bioengineering, School of Life Sciences (SV) and School of Engineering (STI), Ecole Polytechnique Fédérale de Lausanne (EPFL), 1015 Lausanne, Switzerland. [2]School of Life Sciences, Core Facility PTECH, EPFL, 1015 Lausanne, Switzerland. [3]Institute of Chemical Sciences and Engineering, School of Basic Science (SB), EPFL, 1015 Lausanne, Switzerland. †These authors contributed equally to this work. *e-mail: matthias.lutolf@epfl.ch

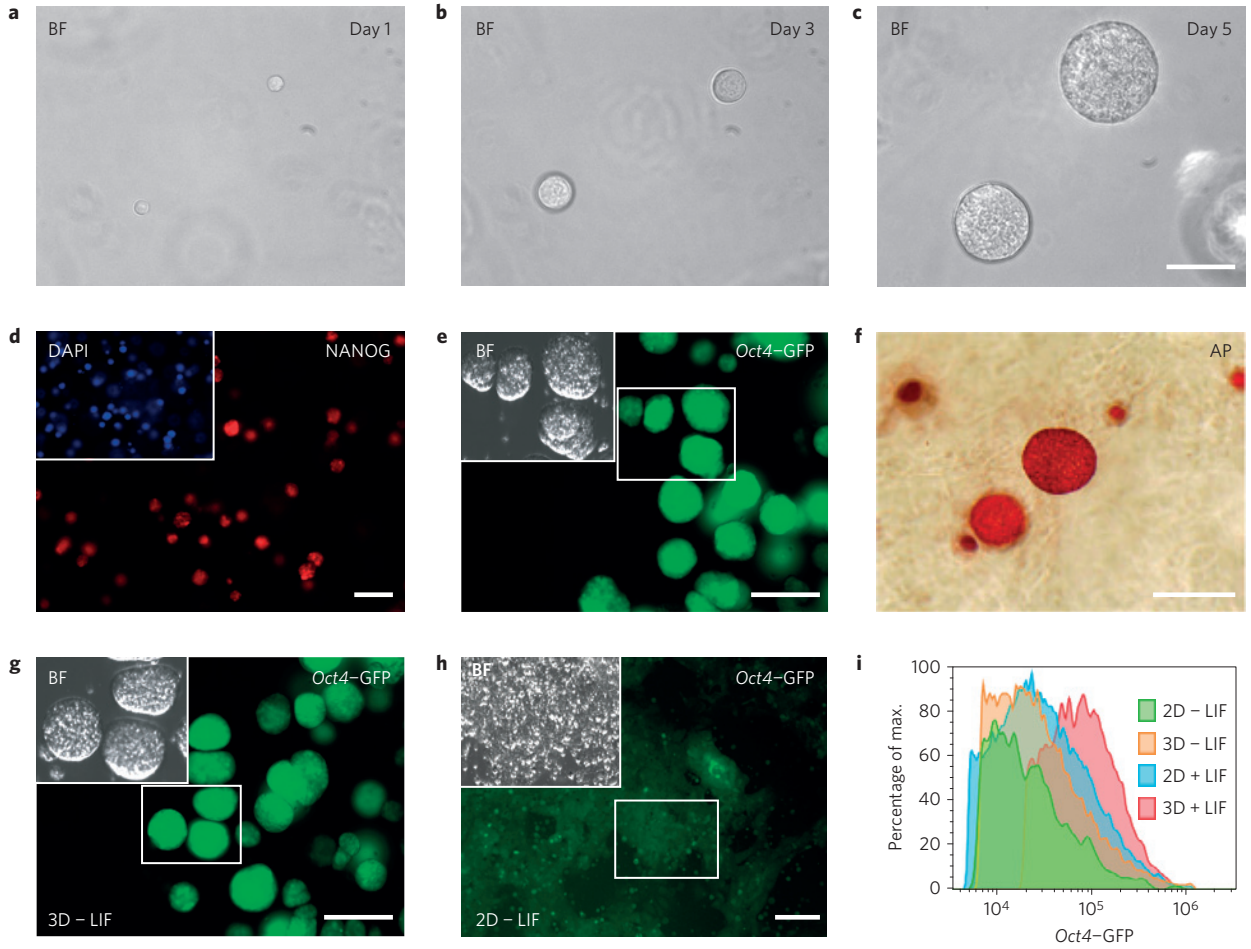

Figure 1 | 3D PEG hydrogel cultures maintain ESC pluripotency. a–c, ESC colony growth 1, 3 and 5 days after encapsulation in PEG hydrogels. BF, bright field. **d**, Immunostaining for NANOG (the inset shows the relative DAPI staining). **e**, *Oct4*-driven GFP expression. **f**, Alkaline phosphatase (AP) staining. **g**,**h**, *Oct4*–GFP expression of ESCs grown without LIF in three dimensions for one week (**g**) or in two dimensions (**h**). Insets show the bright-field images with undifferentiated and differentiated morphologies in 3D and 2D conditions, respectively. **i**, Flow cytometry analysis of *Oct4*–GFP expression of ESCs cultured in 2D and 3D conditions with or without LIF. Scale bars, 100 μm.

and alkaline phosphatase (Fig. 1a–f). Furthermore, Alamar blue assays confirmed sustained viability in PEG-based hydrogels (data not shown). Notably, whereas ESCs cultured in two dimensions rapidly differentiated following LIF removal, 3D-encapsulated cells maintained their typical undifferentiated morphology and *Oct4*–GFP expression as much as nine days after removal of LIF (Fig. 1g–i), suggesting that spatial confinement of cells in the 3D microenvironment plays a role in maintaining pluripotency.

iPSC generation in defined 3D microenvironments

The promising results obtained with 3D ESC culture prompted us to use the same 3D microenvironment formulation for iPSC generation. To assess whether reprogramming to pluripotency could be achieved in a 3D context, we employed a well-defined mouse model system based on the drug-inducible expression of the four Yamanaka factors[20] (Fig. 2a). *Pou5f1*$^{tm2(EGFP)}$ mice harbouring an IRES–EGFP fusion cassette downstream of the stop codon of the *Oct4* gene[21] were crossed with the mutant mice *R26*^{rtTA};*Col1a1*^{4F2A} harbouring both the doxycycline-inducible polycistronic 4F2A cassette (*Oct4*, *Sox2*, *Klf4* and *Cmyc*) and the constitutively expressed reverse tetracycline transactivator (rtTA; ref. 22). We then derived primary tail-tip fibroblasts from the resulting *Pou5f1*$^{tm2(EGFP)}$;*R26*^{rtTA};*Col1a1*^{4F2A} (4F2A–*Oct4*–GFP) mice and encapsulated them in PEG-based hydrogels. Reprogramming was initiated the following day by addition of doxycycline, and the appearance of *Oct4*–GFP+ iPSC colonies in 3D gels, termed '3DiPSCs', was quantified over a period of two weeks. Strikingly, *Oct4*–GFP-expressing colonies began to appear in these 'standard' gels after only six days of doxycycline induction (Supplementary Movie 1). After 16 days of reprogramming and an additional seven days without doxycycline, we found by immunofluorescence staining that 3DiPSCs expressed the main pluripotency markers OCT4, SOX2 and NANOG (Fig. 2b) and showed transcriptional pluripotency signatures comparable to control mouse ESCs and iPSCs generated in 2D culture (Fig. 2c). Moreover, 3DiPSCs could differentiate into all three germ layers *in vitro* (Fig. 2d–f). To further compare the 3DiPSCs with ESCs, we employed bisulphite sequencing to assess the methylation states of CpG dinucleotides in the *Oct4* and *Nanog* promoter regions. These experiments demonstrated that *Oct4* and *Nanog* promoter regions were highly demethylated compared with the parental fibroblasts and possessed methylation states closely resembling those of ESCs (Fig. 2g). Most importantly, 3DiPSCs were competent to generate chimaeric mice (Fig. 2h) and differentiated into all three germ layers in an *in vivo* teratoma assay (Fig. 2i–l).

3D microenvironments enhance reprogramming

After confirming the feasibility of generating iPSCs in 3D culture, we used tail-tip fibroblasts derived from 4F2A–*Oct4*–GFP mice to perform a comparative study with the standard 2D culture protocol.

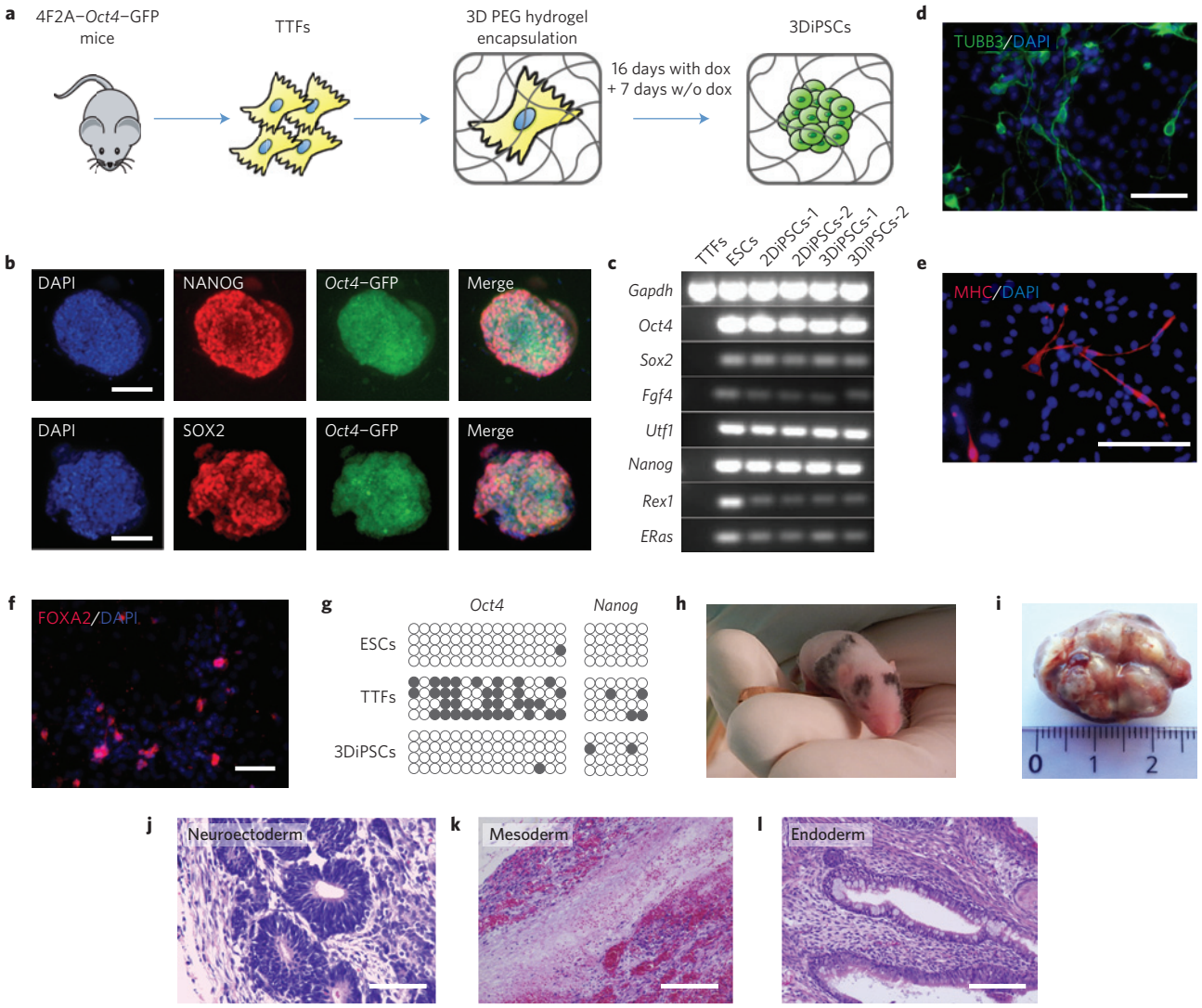

Figure 2 | Generation of 3DiPSCs. a, Schematic representation of the one-step 3D reprogramming protocol. **b**, Immunocytochemistry analysis of pluripotency markers in 3DiPSCs. **c**, RT–PCR analysis of pluripotency marker genes in 2 clones of 3DiPSCs (3DiPSCs-1, 3DiPSCs-2) compared with 2DiPSCs (2DiPSCs-1, 2DiPSCs-2), ESCs and tail-tip fibroblasts (TTFs). **d–f**, Immunostaining showing differentiation of 3DiPSCs into neuroectodermal (TUBB3), mesodermal (MHC, myosin heavy chain) and endodermal (FOXA2) cell types. **g**, Methylation analysis of *Oct4* and *Nanog* promoters in 3DiPSCs, ESCs and tail-tip fibroblasts. **h**, Chimaeric mouse generated with 3DiPSCs. **i–l**, Teratoma assay demonstrating that 3DiPSCs are able to differentiate *in vivo* into neuroectoderm, mesoderm and endoderm. Scale bars, 50 μm (**b**,**d–f**,**k**,**l**) or 25 μm (**j**). dox, doxycycline.

As ESC self-renewal in three dimensions was found to be strongly cell density-dependent (Supplementary Fig. 1g), we first tested how this parameter would influence 3D reprogramming. Indeed, 3D reprogramming was also highly dependent on cell density and, at an optimal density of 500 cells μl^{-1}, was found to result in significantly higher reprogramming efficiency compared with the 2D culture conditions (Fig. 3a).

At the observed optimal cell density, *Oct4*–GFP-expressing colonies began to appear in three dimensions two days earlier than in two dimensions (Fig. 3b,c). To understand how the 3D environment could engender such different reprogramming dynamics and efficiencies, we next compared cell viability and proliferation in 2D and 3D conditions. A LIVE/DEAD analysis by Calcein AM and ethidium homodimer-I staining revealed comparable survival rates (Supplementary Fig. 2a), whereas the proliferation rate assessed by EdU labelling substantially differed (Supplementary Fig. 2b): in two dimensions, fibroblasts proliferate rapidly between day 2 and day 6 followed by a lag phase most likely caused by cell confluence. Cells then re-enter a phase of rapid cell division between day 10 and 14, representing the colony-formation phase indicative of reprogramming. In contrast, cells in 3D culture initially proliferate much slower, but continue to steadily increase their proliferation rate over the course of the experiment. These data suggest that the 3D microenvironment might keep cells in an active proliferative state throughout the entire reprogramming process (Supplementary Fig. 2b–e).

Further analysis of the 3D reprogramming dynamics showed that fibroblasts cultured in PEG hydrogels lost their typical spindle-shaped mesenchymal morphology and formed spherical colonies as early as day 3 (Supplementary Fig. 3a,b). Accordingly, forward scatter analysis by flow cytometry revealed that within the first three days, 3D-encapsulated cells acquire an iPSC-like size, which was stably maintained, whereas most cells in two dimensions reach that size only during the late phase of reprogramming (Supplementary Fig. 3c,d).

To provide further proof of accelerated cell reprogramming in three dimensions, we examined whether differences exist in the temporal requirement of factor expression between the two

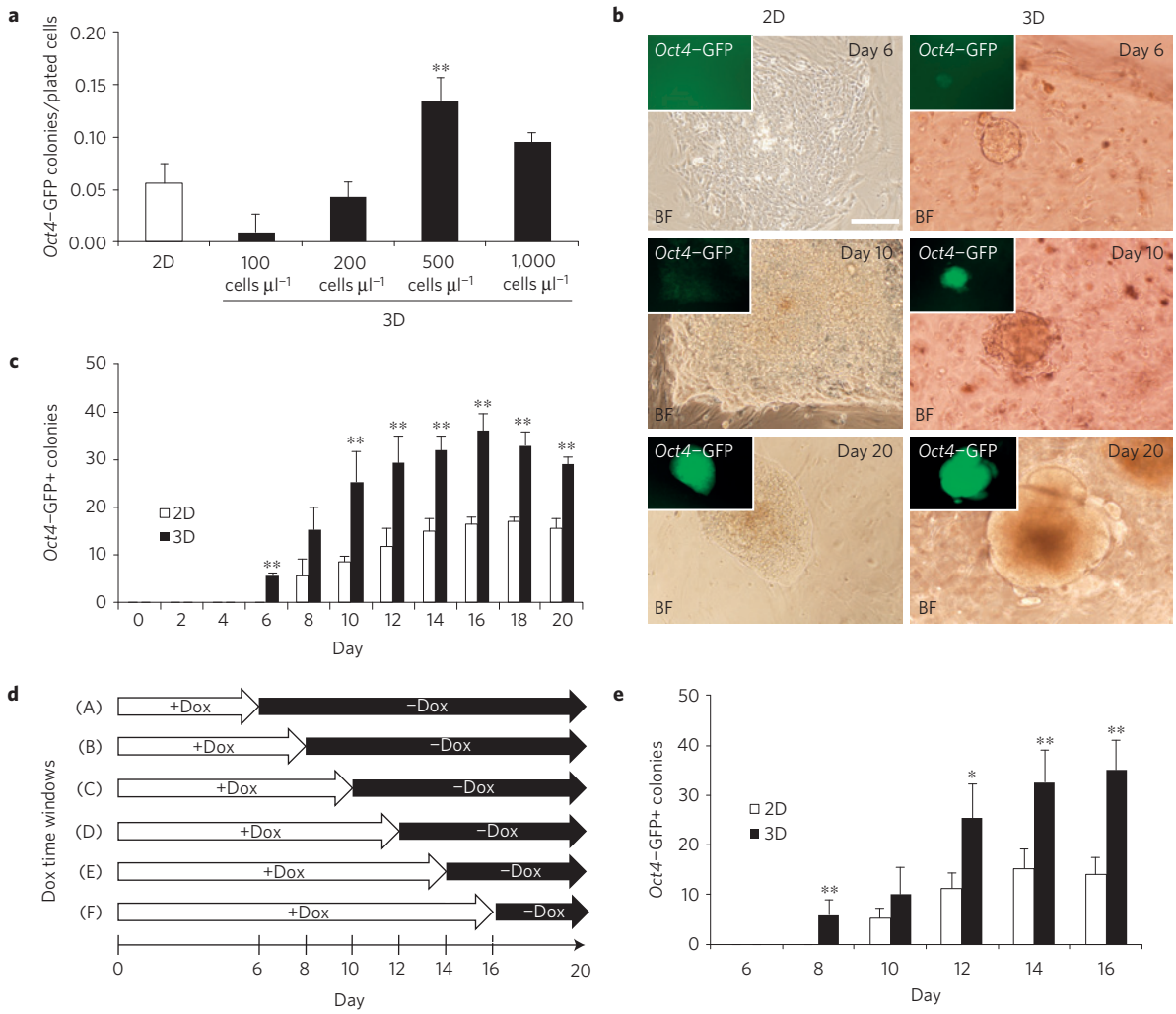

Figure 3 | 3D culture accelerates reprogramming and increases iPSC generation efficiency. a, 3DiPSC generation efficiency obtained with different cell densities. **b**, Representative bright-field images taken during the derivation of 2D and 3DiPS cells showing early colony formation (day 6), *Oct4*-GFP+ colony formation (day 10), and mature, doxycycline-independent iPSC colony formation (day 20) in the 3D condition. Insets show *Oct4*-GFP expression. **c**, Quantification of *Oct4*-GFP+ colonies over the course of the reprogramming process in 2D and 3D conditions. **d**, Experimental design of iPSC stability study. Doxycycline was removed at different time points to determine the kinetics of iPSC generation. **e**, 3D culture accelerates acquisition of independence from exogenous reprogramming factor expression. Data are expressed as means ± s.e.m. **, $p < 0.01$; *, $p < 0.05$. Scale bar, 30 µm. Biological replicates ($n = 6$) are represented in **a**,**c**, and **e**. The same starting number of cells per sample was used in all comparative experiments in 2D and 3D conditions.

conditions. Doxycycline was therefore applied for 6, 8, 10, 12, 14 or 16 days on reprogramming fibroblasts (Fig. 3d). Strikingly, in three dimensions, an 8-day doxycyline treatment was already sufficient to give rise to iPSCs, in contrast to two dimensions (Fig. 3e), providing evidence for the faster induction of iPSCs in 3D culture.

Optimization of iPSC generation by 3D artificial niches

Our previous experiments showed that a 3D microenvironment can strongly affect iPSC generation when optimized for the maintenance of ESC pluripotency in three dimensions. However, as fibroblast and early iPSC states might require significantly different 3D matrix characteristics, we postulated that an optimization of this 'standard' 3D matrix composition might further improve reprogramming efficacy. To test this, we took advantage of the tunable nature of our artificial ECM platform to systematically probe how biophysical and biochemical cues could influence reprogramming (Fig. 4).

To this end, we employed a previously developed 3D high-throughput screening (HTS) approach[19] to simultaneously probe 128 unique microenvironmental conditions in triplicate. Using an automatic high-throughput imaging system we were able to detect the number, phenotype and *Oct4*–GFP intensities of colonies in response to each microenvironment (Fig. 4a). We used this approach to tune matrix stiffness between 300 and 1,200 Pa (G') and explore the susceptibility of the gel to MMP degradation using gel building blocks with high or intermediate degree of degradability. Furthermore, we reasoned that we could improve the induction of iPSCs by enriching PEG hydrogels with proteins previously shown to play a role in regulating pluripotency. Thus, we selected and screened several cell–cell interactions and ECM proteins, namely E-cadherin[23], Epcam[24], laminin[25], fibronectin[26] (and its minimal signalling peptide RGD and fragment F9-10), vitronectin[27] and collagen IV (ref. 28). Finally, we analysed the synergistic effect of Wnt pathway stimulation, achieved here by the GSK3β inhibitor CHIR99021, which is also known to contribute to pluripotency induction[29]. The complete list of the 128 screened conditions is reported in Supplementary Table 1.

The outcome of this HTS showed that our previously used 'standard' 3D condition could be largely improved on. Indeed our 'standard' condition (marked by the yellow bar in Fig. 4b) was in the lower half of all conditions, ranked by the number of identified

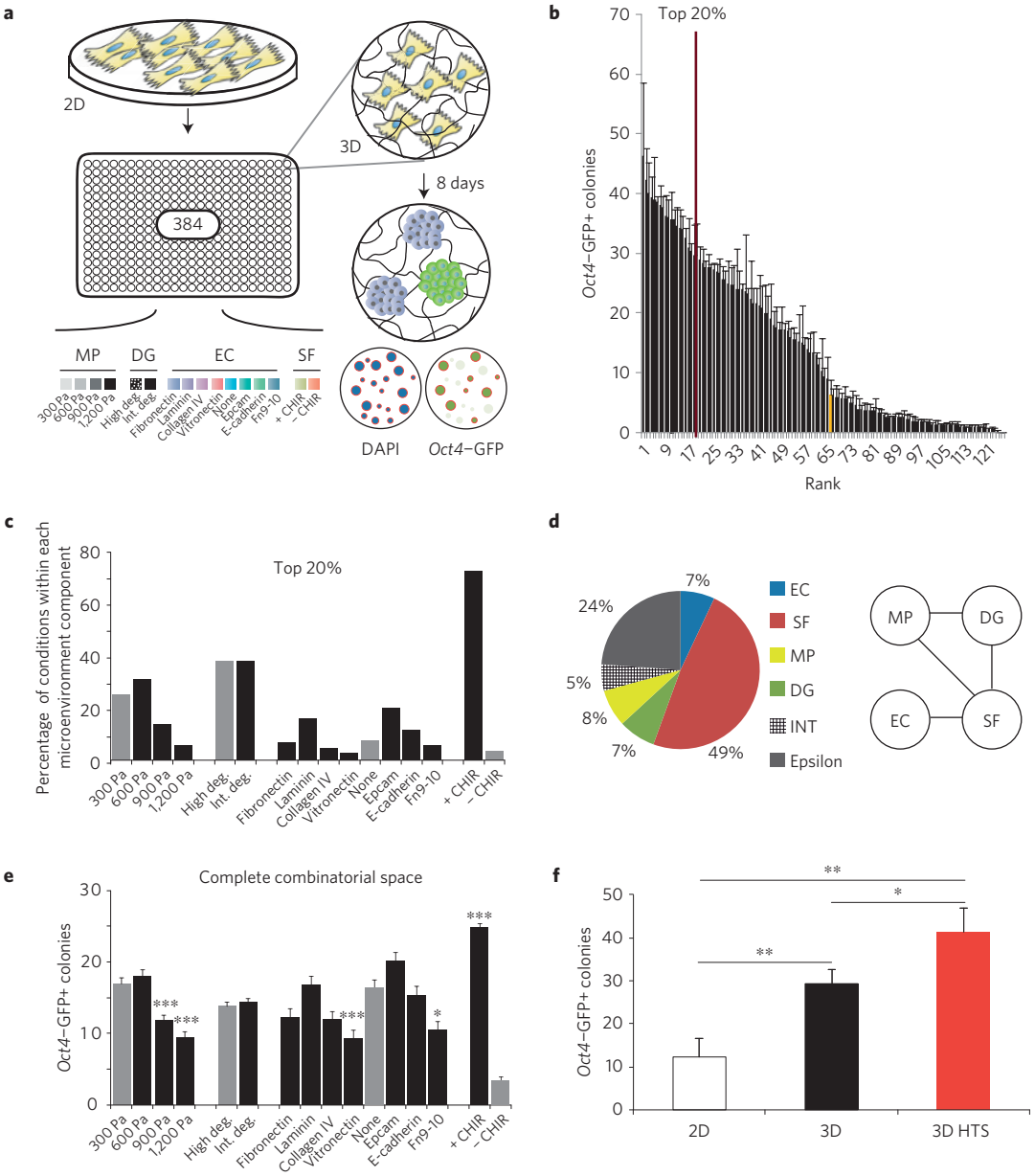

Figure 4 | Optimization of iPSC reprogramming efficiency by modulation of 3D microenvironment. a, 3D HTS approach to simultaneously probe 128 unique microenvironmental conditions (in triplicate). Read-outs: number, phenotype and *Oct4*-GFP intensities of colonies in response to each microenvironment. **b**, Quantification of *Oct4*-GFP-positive colonies in all 128 unique conditions analysed by HTS in 3D PEG hydrogels. Yellow bar indicates the 'standard' 3D condition. **c**, Microenvironmental components within the identified top 20% unique conditions. **d**, Relative contribution and interactions of component categories to global regulatory landscape (MP, mechanical properties; DG, degradability (MMP sensitivity); SF, soluble factors; EC, extracellular matrix and cell–cell contact proteins; INT, interactions; Epsilon, model uncertainty). **e**, Global analysis of individual component contributions to reprogramming efficiency. **f**, Comparison of reprogramming efficiency in HTS-derived condition versus standard 3D and 2D conditions. Data are expressed as means ± s.e.m. All pairwise differences were computed using the Tukey–Kramer method. ***, $p < 0.001$; **, $p < 0.01$; $p < 0.05$. Biological replicates ($n = 5$) are represented in **e**.

Oct4–GFP-positive colonies. A detailed analysis of the top 20% conditions clearly highlighted that the ideal stiffness occurred between 300 and 600 Pa and that enrichment of the microenvironment with Laminin or Epcam resulted in marked improvements in 3DiPSC generation. Notably, we also observed a strong correlation between the activation of the Wnt pathway by CHIR99021 and reprogramming efficiency in three dimensions (Fig. 4c).

We then performed a comprehensive quantitative analysis of *Oct4*–GFP expression and an image-based assessment of morphological parameters of the colonies detected by high-throughput imaging and grouped all of the conditions by hierarchical clustering (Supplementary Fig. 5a). This analysis confirmed that our automated identification of the number of GFP-positive colonies correlated with manual image assessment. Furthermore, it identified colony area as being closely correlated to GFP-positive colony number, indicating that conditions of high proliferation would be favourable to reprogramming. Interestingly, colony morphology and GFP intensity were not closely correlated with the appearance of *Oct4*–GFP-positive colonies, suggesting that 3D reprogramming efficiency was decoupled from levels of *Oct4*–GFP expression and colony shape. To investigate the conditions leading to the identified clustered patterns, we further assessed selected clusters with the

highest and lowest reprogramming efficiency and discovered that they resulted from highly divergent microenvironmental conditions (Supplementary Fig. 5b,c).

To quantify the relative contribution of the various microenvironmental categories to reprogramming efficiency as well as to identify significant interactions between these microenvironmental categories, we created a generalized linear model (GLM; see Methods) relating *Oct4*–GFP colony efficiency to all 128 input conditions (Fig. 4d). This analysis also permitted us to identify the global landscape of contributions of individual factors to reprogramming efficiency, clearly identifying global positive and negative regulators of reprogramming and corroborating the optimal parameters arising from the identified top 20% conditions (Fig. 4e). To validate these results, we replicated in 12-well plate culture the best condition of the 3D microenvironment screening (that is, 600 Pa, high degradability, gel enriched with Epcam, and CHIR) together with the previously used 'standard' condition. This experiment confirmed that fine-tuning a defined 3D microenvironment can further increase iPSC generation: compared with the standard protocol in 2D our 3D approach resulted in a more than threefold increase in reprogramming efficiency (Fig. 4f).

Finally, we sought to compare our 3D reprogramming conditions in chemically defined microenvironments with other 3D culture techniques. Therefore, we compared the efficiency of reprogramming in cells encapsulated in our 'standard' PEG gels, Matrigel and collagen type I gels, and a previously published biophysical reprogramming method based on microgrooves[15]. Our results showed that 3D PEG-based hydrogels are able to support the generation of a significantly higher number of *Oct4*–GFP-positive colonies compared with collagen I or microgrooves (Supplementary Fig. 4a). Interestingly, 3D Matrigel also significantly increased iPSC generation to a level comparable to our 'standard' 3D PEG hydrogels (Supplementary Fig. 4a). However, neither collagen nor Matrigel supported the generation of iPSC colonies with a homogeneous morphology (Supplementary Fig. 4b–e). We believe that the relatively rapid degradation and variable formulation of naturally derived hydrogel systems such as collagen and Matrigel substantially limit the potential use of these 3D culture methods compared with our chemically defined system.

Taken together, these data demonstrate that the modulation of the 3D microenvironment is crucial to obtain reprogramming efficiencies that may be unachievable with 2D or other 3D culture methods in which cell–matrix perturbations are limited.

3D culture promotes MET and epigenetic plasticity

We next focused on elucidating the mechanisms that underlie the significant differences observed between cell reprogramming in 2D and 3D conditions. To this end, we began by analysing Yes-associated protein (YAP) signalling, one of main pathways regulating stem cell fate choices induced by physical inputs[30], with a previously documented role during reprogramming to pluripotency[31]. Surprisingly, we did not find any evident sign of nuclear YAP1 activity by immunohistochemistry for 3D reprogramming in early colonies (that is, at day 8, Supplementary Fig. 6a–c). However, we noted that at the onset of reprogramming (day 1–3), a substantial fraction of fibroblasts in two dimensions expressed nuclear YAP1, whereas in 3D hydrogels this phenotype was never observed (Supplementary Fig. 6d,e). Consistently, at these time points the expression of YAP1 target genes (*Ankrd1*, *Ctgf* and *Cyr61*) in three dimensions was much weaker compared with 2D controls (Supplementary Fig. 6g–i). This differential YAP1 activity on surfaces versus 3D hydrogels at the beginning of reprogramming, when cells are still 'fibroblast-like', is consistent with the work of Piccolo and colleagues, which has shown nuclear YAP/TAZ activity for cells on hard substrates (or large adhesive islands) and cytoplasmic, inactive YAP/TAZ for those on soft hydrogels (or small adhesive islands)[30]. These results could indicate that YAP/TAZ modulation may also play a role in the early phases of reprogramming, as has already been shown for Wnt pathway activity[32], which is known to be linked to YAP/TAZ (ref. 33). The extent and mechanisms to which these early differences in YAP activity explain our reprogramming results clearly require further elucidation.

A detailed confocal microscopy-based assessment of the morphological changes during early reprogramming provided evidence that 3D conditions favoured the formation of colony-like structures after only three days of doxycycline exposure (Supplementary Fig. 3, and data not shown). The pronounced change in the shape of fibroblasts towards a round morphology within the first three days of 3D reprogramming suggested that the matrix induced the cells to undergo an apparent phenotypic change to an epithelial-like morphology. Indeed, MET is a key initiation step during the generation of iPSCs and is instrumental for colony formation[34,35]. We therefore analysed the transcripts of key MET markers during the reprogramming process (Fig. 5a–c) and found that a 3D microenvironment accelerates the expression of epithelial markers (E-cadherin and *Epcam*) and results in a concomitant loss of the fibroblast phenotype (*Thy1*). Accordingly, immunocytochemical analysis highlighted that E-cadherin protein appears much earlier in 3D (day 3) than in 2D culture (day 5) (Fig. 5d–f and data not shown). These data suggest that the 3D microenvironment accelerates iPSC generation through an earlier induction of the MET process.

We next asked whether the observed rapid changes in cell morphology and size in 3D culture are accompanied by rearrangements in chromatin structure. Histone acetylation and methylation were chosen here as candidates for histone marks because their role in iPSC generation has been extensively studied[36]. In particular, tri-methylation at lysine 4 of histone H3 (H3K4me3) has been identified to play a role in the activation of genes responsible for proliferation and metabolism during the early phase of reprogramming[37]. Furthermore, reduction in H3K4me3 levels in mouse ESCs has been demonstrated to cause attenuated expression of self-renewal markers including OCT4, NANOG and SSEA1 (ref. 38), highlighting its importance in the maintenance of pluripotency. Histone H3 acetylation (AcH3) is also critical for cell reprogramming, as it marks open chromatin and thus promotes active transcription. Accordingly, histone deacetylase inhibitors such as valproic acid improve iPSC generation efficiency and allow successful reprogramming in the absence of c-Myc and Klf4 (ref. 39). Therefore, we monitored by immunofluorescence and image analysis AcH3 and H3K4me3 levels during the early phase (day 3) of 2D and 3D reprogramming. Interestingly, we observed a significant increase in H3K4me3 levels in the 3D relative to the 2D culture condition as well as an increase in the AcH3 mark in 3D culture (Fig. 5g, left panels). A similar trend in histone modifications was observed even in fibroblasts cultured without doxycycline induction (Fig. 5g, right panels), a result that was confirmed by western blot analysis (Fig. 5h). However, H3K4me3 and AcH3 protein increases were not detectable in 3D samples treated with doxycycline, possibly because these epigenetic markers were already strongly induced by the reprogramming factors. Taken together, these data show that the exposure of single cells to a 3D microenvironment induces marked changes in chromatin structure, which is well known to be essential for overcoming the epigenetic barriers of cell reprogramming.

3D culture promotes pluripotency induction in human cells

Our final aim was to test whether iPSCs could be generated in a 3D microenvironment by reprogramming of human somatic cells. Therefore, we tried to reprogramme human fibroblasts into iPSCs using a lentiviral vector-based approach, comparing 2D and our 3D

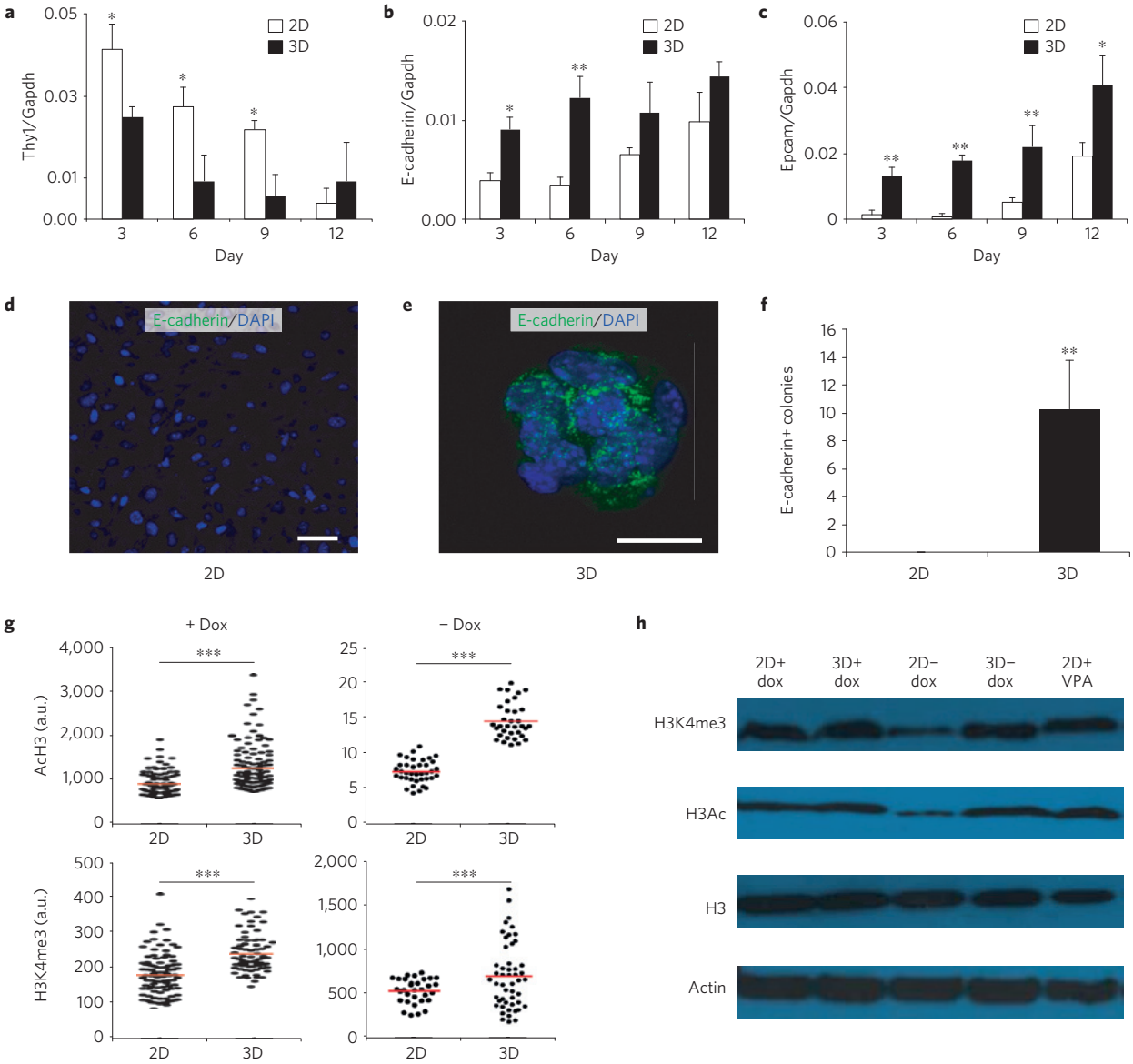

Figure 5 | 3D reprogramming accelerates MET and enhances epigenetic plasticity. a–c, Real-time RT–PCR analysis of MET markers during 2D and 3D reprogramming. Transcripts were normalized to *Gapdh* levels. **d–f**, Immunocytochemical analysis for E-cadherin in 2D or 3D culture conditions after 3 days of reprogramming and relative quantification. **g**, Cells cultured for 3 days in 2D and 3D conditions with or without doxycycline (dox) induction were fixed and stained for AcH3 or H3K4me3 and signal intensity was quantified by image analysis. **h**, Western blot analysis of epigenetic marks in 2D and 3D conditions. Valproic acid (VPA, 0.5 mM) was used as a positive control. Data are expressed as means ± s.e.m. ***, $p < 0.001$; **, $p < 0,01$; *, $p < 0.05$. Scale bars, 30 μm. Biological replicates ($n = 3$) are represented in **a–c** and ($n = 6$) **f**.

PEG-hydrogel-based protocols. Both 'standard' and HTS-optimized 3D conditions were able to accelerate human iPSC generation. NANOG expression became detectable in three dimensions after only 14 days of reprogramming, whereas it was undetectable in standard 2D conditions at that relatively early time point (Fig. 6a and data not shown). Moreover, after 6 weeks of reprogramming, the efficiency of human 3DiPSC generation was found to be up to 2.5-fold higher in 3D culture (Fig. 6b). Human 3DiPSCs showed a mature morphology (Fig. 6c) and expressed SOX2, NANOG, OCT4 and SSEA-4, the cardinal markers of human pluripotency (Fig. 6d–g). Pluripotency of the reprogrammed human cells was further corroborated by multilineage *in vitro* differentiation (Fig. 6h–j) and *in vivo* teratoma formation (Fig. 6k–n). These results demonstrate that an engineered 3D cell microenvironment can also be deployed to enhance human reprogramming, thereby opening up our method for translational applications.

Recently, several research groups have investigated 3D culture systems to identify extrinsic factors meditating ESC pluripotency (for example, refs 40–44). To the best of our knowledge, there are no complementary studies exploring the generation of iPSCs in 3D microenvironments. Our PEG-based hydrogel system represents a powerful model system to dissect the role of microenvironmental signals in modulating cell reprogramming. Whereas current 2D methods may limit iPSC generation owing to rapid cell confluency, the 3D method we present here overcomes this issue by promoting proliferation throughout the entire reprogramming process. Our results suggest that the 3D matrix selects for colony-forming iPSCs because the proliferation of non-colony-forming cells is limited in the 3D milieu. Notably, compared with reprogramming in conventional 2D conditions, reprogramming kinetics and efficiency are improved in three dimensions, most likely caused by the action of biophysical cues from the 3D microenvironment that may

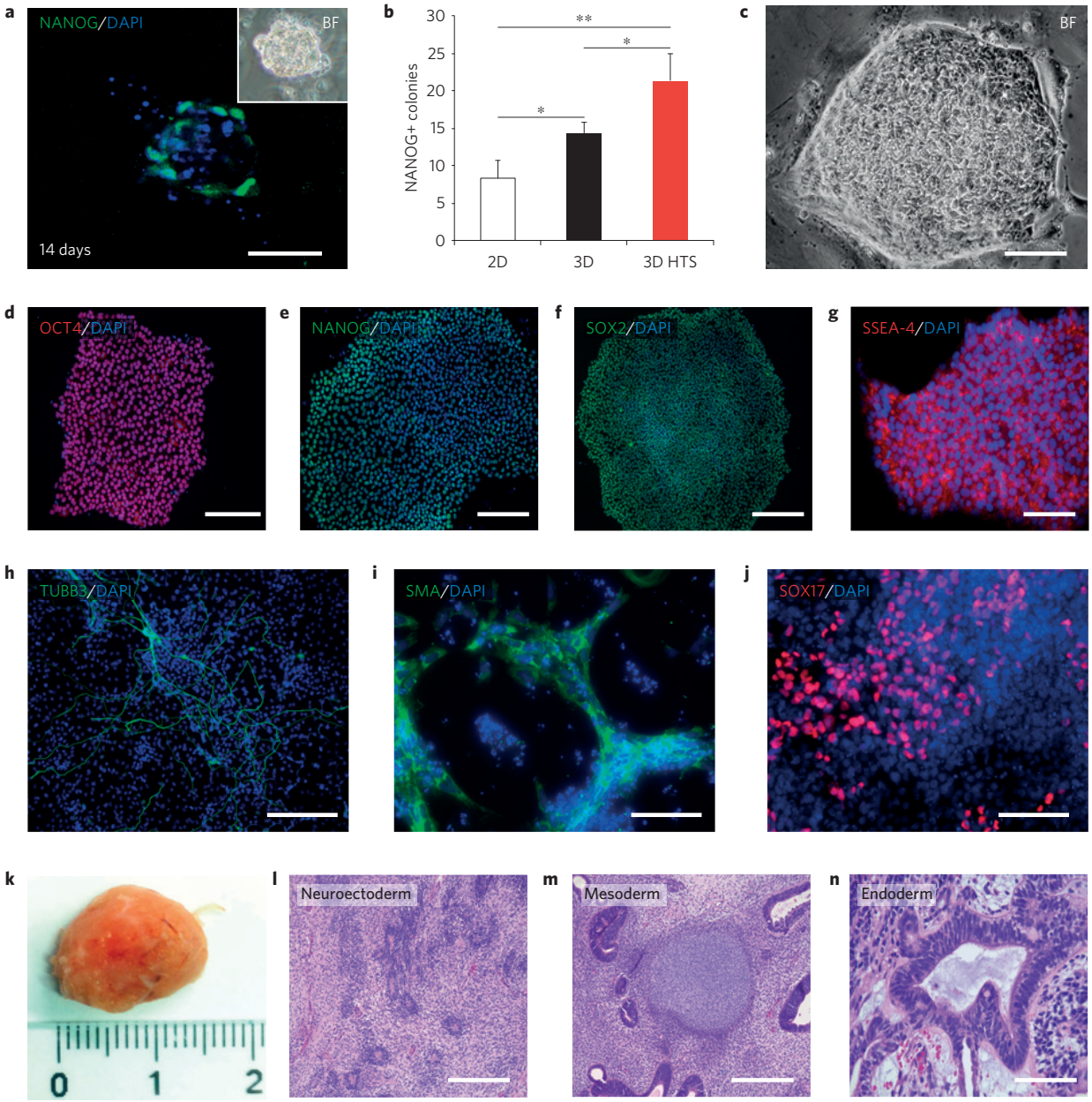

Figure 6 | 3D generation of human iPSCs. a, Immunostaining for NANOG after 14 days of 3D reprogramming. Inset shows the corresponding bright-field image (BF). **b**, Comparison of reprogramming efficiency in 2D and 3D culture ('standard' and conditions optimized by HTS). **c**, Human 3DiPSC colony after 6 weeks of reprogramming. **d**–**g**, Immunocytochemistry analysis of pluripotency markers in human 3DiPSCs. **h**–**j**, Immunostaining showing differentiation of human 3DiPSCs into neuroectodermal (TUBB3), mesodermal (SMA, smooth muscle actin) and endodermal (SOX17) cell types. **k**–**n**, Teratoma assay showing that human 3DiPSCs are able to differentiate *in vivo* into neuroectoderm, mesoderm and endoderm. Data are shown as means ± s.e.m. **, $p < 0,01$; *, $p < 0.05$. Biological replicates ($n = 5$) are represented in **a**–**c**. Scale bars, 30 μm (**a**,**n**), 100 μm (**c**–**h**,**l**,**m**) or 50 μm (**i**,**j**). The same starting number of cells per sample was used in the comparative experiment (**b**) in 2D and 3D conditions.

cooperate with the induced transcription factors. We also note that the observed cell confinement and controlled proliferation make our approach particularly attractive for the scalable, automatized generation of iPSCs, which is difficult to implement with standard 2D methods.

Our experiments show that early events during 3D reprogramming are accompanied by pronounced morphological changes that may cause both chromatin remodelling and accelerated MET, two key events for the initiation of iPSC generation. Consistent with the idea that the 3D environment can have a profound effect on cell reprogramming, we observed higher levels of AcH3 and H3K4me3 in 3D conditions even without transgene overexpression (Fig. 5c,d). Interestingly, our data are in accordance with previously published work showing that biophysical stress can modulate the epigenetic state in cell reprogramming[15].

Our findings represent a first proof of principle for 3D reprogramming and pave the way for further investigations into the discovery of a synthetic 'reprogramming niche'. This concept opens up the intriguing possibility of shifting from genetic to microenvironmental manipulations of somatic cell fate, which would be of particular interest for clinical applications of iPSC technology. Furtheremore, model systems such as those used in this work could help achieve a deeper understanding of cell-extrinsic factors involved in cell fate regulation.

Methods

Methods and any associated references are available in the online version of the paper.

Received 5 February 2015; accepted 8 December 2015; published online 11 January 2016

References

1. Ben-Ze'ev, A., Farmer, S. R. & Penman, S. Protein synthesis requires cell-surface contact while nuclear events respond to cell shape in anchorage-dependent fibroblasts. *Cell* **21,** 365–372 (1980).
2. Chen, C. S., Mrksich, M., Huang, S., Whitesides, G. M. & Ingber, D. E. Geometric control of cell life and death. *Science* **276,** 1425–1428 (1997).
3. Chowdhury, F. *et al.* Material properties of the cell dictate stress-induced spreading and differentiation in embryonic stem cells. *Nature Mater.* **9,** 82–88 (2010).
4. Engler, A. J., Sen, S., Sweeney, H. L. & Discher, D. E. Matrix elasticity directs stem cell lineage specification. *Cell* **126,** 677–689 (2006).
5. Lutolf, M. P. & Hubbell, J. A. Synthetic biomaterials as instructive extracellular microenvironments for morphogenesis in tissue engineering. *Nature Biotechnol.* **23,** 47–55 (2005).
6. Singhvi, R. *et al.* Engineering cell shape and function. *Science* **264,** 696–698 (1994).
7. Thomas, C. H., Collier, J. H., Sfeir, C. S. & Healy, K. E. Engineering gene expression and protein synthesis by modulation of nuclear shape. *Proc. Natl Acad. Sci. USA* **99,** 1972–1977 (2002).
8. Bissell, M. J., Rizki, A. & Mian, I. S. Tissue architecture: the ultimate regulator of breast epithelial function. *Curr. Opin. Cell Biol.* **15,** 753–762 (2003).
9. Roskelley, C. D., Desprez, P. Y. & Bissell, M. J. Extracellular matrix-dependent tissue-specific gene expression in mammary epithelial cells requires both physical and biochemical signal transduction. *Proc. Natl Acad. Sci. USA* **91,** 12378–12382 (1994).
10. Streuli, C. H. *et al.* Laminin mediates tissue-specific gene expression in mammary epithelia. *J. Cell. Biol.* **129,** 591–603 (1995).
11. Grant, P. A. A tale of histone modifications. *Genome Biol.* **2,** http://dx.doi.org/10.1186/gb-2001-2-4-reviews0003 (2001).
12. Sancho-Martinez, I. & Izpisua Belmonte, J. C. Stem cells: surf the waves of reprogramming. *Nature* **493,** 310–311 (2013).
13. Polo, J. M. *et al.* A molecular roadmap of reprogramming somatic cells into iPS cells. *Cell* **151,** 1617–1632 (2012).
14. Hansson, J. *et al.* Highly coordinated proteome dynamics during reprogramming of somatic cells to pluripotency. *Cell. Rep.* **2,** 1579–1592 (2012).
15. Downing, T. L. *et al.* Biophysical regulation of epigenetic state and cell reprogramming. *Nature Mater.* **12,** 1154–1162 (2013).
16. Ehrbar, M. *et al.* Enzymatic formation of modular cell-instructive fibrin analogs for tissue engineering. *Biomaterials* **28,** 3856–3866 (2007).
17. Ehrbar, M. *et al.* Biomolecular hydrogels formed and degraded via site-specific enzymatic reactions. *Biomacromolecules* **8,** 3000–3007 (2007).
18. Ehrbar, M. *et al.* Elucidating the role of matrix stiffness in 3D cell migration and remodeling. *Biophys. J.* **100,** 284–293 (2011).
19. Ranga, A. *et al.* 3D niche microarrays for systems-level analyses of cell fate. *Nature Commun.* **5,** 4324 (2014).
20. Takahashi, K. & Yamanaka, S. Induction of pluripotent stem cells from mouse embryonic and adult fibroblast cultures by defined factors. *Cell* **126,** 663–676 (2006).
21. Lengner, C. J. *et al.* Oct4 expression is not required for mouse somatic stem cell self-renewal. *Cell Stem Cell* **1,** 403–415 (2007).
22. Markoulaki, S. *et al.* Transgenic mice with defined combinations of drug-inducible reprogramming factors. *Nature Biotechnol.* **27,** 169–171 (2009).
23. Hawkins, K., Mohamet, L., Ritson, S., Merry, C. L. & Ward, C. M. E-cadherin and, in its absence, N-cadherin promotes Nanog expression in mouse embryonic stem cells via STAT3 phosphorylation. *Stem Cells* **30,** 1842–1851 (2012).
24. Gonzalez, B., Denzel, S., Mack, B., Conrad, M. & Gires, O. EpCAM is involved in maintenance of the murine embryonic stem cell phenotype. *Stem Cells* **27,** 1782–1791 (2009).
25. Domogatskaya, A., Rodin, S., Boutaud, A. & Tryggvason, K. Laminin-511 but not -332, -111, or -411 enables mouse embryonic stem cell self-renewal *in vitro*. *Stem Cells* **26,** 2800–2809 (2008).
26. Soteriou, D. *et al.* Comparative proteomic analysis of supportive and unsupportive extracellular matrix substrates for human embryonic stem cell maintenance. *J. Biol. Chem.* **288,** 18716–18731 (2013).
27. Braam, S. R. *et al.* Recombinant vitronectin is a functionally defined substrate that supports human embryonic stem cell self-renewal via alphavbeta5 integrin. *Stem Cells* **26,** 2257–2265 (2008).
28. Hayashi, Y. *et al.* Integrins regulate mouse embryonic stem cell self-renewal. *Stem Cells* **25,** 3005–3015 (2007).
29. Marson, A. *et al.* Wnt signaling promotes reprogramming of somatic cells to pluripotency. *Cell Stem Cell* **3,** 132–135 (2008).
30. Dupont, S. *et al.* Role of YAP/TAZ in mechanotransduction. *Nature* **474,** 179–183 (2011).
31. Lian, I. *et al.* The role of YAP transcription coactivator in regulating stem cell self-renewal and differentiation. *Genes Dev.* **24,** 1106–1118 (2010).
32. Aulicino, F., Theka, I., Ombrato, L., Lluis, F. & Cosma, M. P. Temporal perturbation of the Wnt signaling pathway in the control of cell reprogramming is modulated by TCF1. *Stem Cell Rep.* **2,** 707–720 (2014).
33. Azzolin, L. *et al.* Role of TAZ as mediator of Wnt signaling. *Cell* **151,** 1443–1456 (2012).
34. Li, R. *et al.* A mesenchymal-to-epithelial transition initiates and is required for the nuclear reprogramming of mouse fibroblasts. *Cell Stem Cell* **7,** 51–63 (2010).
35. Samavarchi-Tehrani, P. *et al.* Functional genomics reveals a BMP-driven mesenchymal-to-epithelial transition in the initiation of somatic cell reprogramming. *Cell Stem Cell* **7,** 64–77 (2010).
36. Schmidt, R. & Plath, K. The roles of the reprogramming factors Oct4, Sox2 and Klf4 in resetting the somatic cell epigenome during induced pluripotent stem cell generation. *Genome Biol.* **13,** 251 (2012).
37. Koche, R. P. *et al.* Reprogramming factor expression initiates widespread targeted chromatin remodeling. *Cell Stem Cell* **8,** 96–105 (2011).
38. Ang, Y. S. *et al.* Wdr5 mediates self-renewal and reprogramming via the embryonic stem cell core transcriptional network. *Cell* **145,** 183–197 (2011).
39. Huangfu, D. *et al.* Induction of pluripotent stem cells from primary human fibroblasts with only Oct4 and Sox2. *Nature Biotechnol.* **26,** 1269–1275 (2008).
40. Gerecht, S. *et al.* Hyaluronic acid hydrogel for controlled self-renewal and differentiation of human embryonic stem cells. *Proc. Natl Acad. Sci. USA* **104,** 11298–11303 (2007).
41. Lee, S. T. *et al.* Engineering integrin signaling for promoting embryonic stem cell self-renewal in a precisely defined niche. *Biomaterials* **31,** 1219–1226 (2010).
42. Lee, S. T. *et al.* Long-term maintenance of mouse embryonic stem cell pluripotency by manipulating integrin signaling within 3D scaffolds without active Stat3. *Biomaterials* **33,** 8934–8942 (2012).
43. Siti-Ismail, N., Bishop, A. E., Polak, J. M. & Mantalaris, A. The benefit of human embryonic stem cell encapsulation for prolonged feeder-free maintenance. *Biomaterials* **29,** 3946–3952 (2008).
44. Lei, Y. & Schaffer, D. V. A fully defined and scalable 3D culture system for human pluripotent stem cell expansion and differentiation. *Proc. Natl Acad. Sci. USA* **110,** E5039–5048 (2013).

Acknowledgements

We thank M. Snyder and M. Knobloch for critical reading of the manuscript, A. Negro for polymer batch testing, D. Trono for providing *Oct4*–GFP and OKSM-doxy-inducible mice, M. Friedli for providing SFFV-OKSM lentiviral vector and for helpful discussion, M. Pluchinotta and P. Manti for the anti-E-Cad and anti-SMA antibodies, the EPFL Transgenic Core Facilities for generating chimaeric mice, and the EPFL Histology Core Facility for performing teratoma histology. This work was financially supported by the EU framework 7 HEALTH research programme PluriMes (http://www.plurimes.eu), the SystemsX.ch RTD project StoNets, an ERC grant (StG_311422) and a Swiss National Science Foundation Singergia grant (CRSII3_147684).

Author contributions

M.P.L., Y.O. and M.C. designed the experiments and analysed the data. Y.O. and M.C. performed most of the experiments and statistical analyses. M.P.L. and M.C. wrote the manuscript. A.R. performed and analysed the HTS experiment and contributed to manuscript writing. Y.T. fabricated the microgroove platform. A.P. analysed teratoma assays.

Additional information

Supplementary information is available in the online version of the paper. Reprints and permissions information is available online at www.nature.com/reprints. Correspondence and requests for materials should be addressed to M.P.L.

Competing financial interests

The authors declare no competing financial interests.

Methods

Mice. B6;129S4–*Pou5f1*^{tm2Jae} and Gt(ROSA)26Sor$^{tm1(rTA*M2)Jae}$ Col1a1$^{tm3(tetO-Pou5f1,-Sox2,-Klf4-Myc)Jae}$ mice were purchased from The Jackson Laboratory, bred to obtain B6;129S4–*Pou5f1*^{tm2Jae}/Gt(ROSA)26Sor$^{tm1(rTA*M2)Jae}$ Col1a1$^{tm3(tetO-Pou5f1,-Sox2,-Klf4-Myc)Jae}$ (4F2A–*Oct4*–GFP) mice and maintained in micro-isolator cages. Mice were provided continuously with sterile food, water and bedding. All *in vivo* procedures were carried out in accordance with institutional guidelines of Canton Vaud.

Mouse ESC culture. *Oct4*–GFP mouse ESCs (R1) were maintained on 0.2% gelatin-coated tissue culture plates in mouse ESC medium: Dulbecco's modified Eagle's medium (DMEM) supplemented with 2 mM GlutaMAX, 15% (v/v) ESC-qualified fetal bovine serum (FBS; Fisher Scientific), 1 mM sodium pyruvate (Life Technologies), ×1 non-essential amino acids (Gibco), 1% (v/v) penicillin/streptomycin (Gibco), 0.1 mM 2-mercaptoethanol (Gibco), and 103 U ml^{-1} mouse leukaemia inhibitory factor (LIF; Millipore). Medium was stored at 4 °C and was used within 2 weeks.

Isolation and culture of tail-tip fibroblasts. Tail-tip fibroblasts (TTFs) were isolated from 4F2A–*Oct4*–GFP mice. ∼1 cm tail tips were cut from euthanized 8-week-old mice. Dermis was peeled off from the tails, and the remaining tissues were minced into small pieces and incubated in 0.1% trypsin (Invitrogen) for 30 min at 37 °C. Digested tissues were neutralized with FBS, collected by centrifugation (×300*g* for 5 min), and placed onto 0.2% gelatin-coated tissue culture plates in fibroblast medium consisting of Dulbecco's modified Eagle's medium (DMEM) supplemented with 2 mM GlutaMAX, 10% (v/v) fetal bovine serum (FBS; Life Technologies), 1 mM sodium pyruvate (Life Technologies), ×1 non-essential amino acids (Life Technologies), 1% (v/v) penicillin/streptomycin (Life Technologies). Fibroblasts were allowed to migrate out for 7 days. TrypLE Express (Life Technologies) was used for routine passaging TTFs. All cells were cryopreserved at passage 1 and were used exclusively at passage 3 for all experiments.

Cell reprogramming. To reprogramme in adherent 2D conditions, 3×10^4 primary TTFs were plated on 0.2% gelatin-coated 12-well plates. To reprogramme in 3D conditions, primary TTFs were mixed with gel precursors (see below). Crosslinking was performed in 50 mM Tris buffered saline (TBS): 50 mM Tris, 50 mM $CaCl_2$, pH 7.6, and 10 U ml^{-1} thrombin-activated factor XIIIa, conditions that have been previously reported as suitable for 3D cell encapsulation[16]. Hydrogels were formulated in a 12-well plate (1 drop per well) in 30 µl drops using 1,000 cells µl^{-1}. Crosslinking was carried out for 30 min at 37 °C in a humidified incubator. The day after encapsulation, cells were shifted to mouse ESC medium containing 2 µg ml^{-1} doxycycline (Sigma-Aldrich) and medium exchange was carried out every 48 h during the entire reprogramming process.

PEG hydrogels. For convenience, we reproduce below methodological details originally available in refs 17,18. Briefly, the factor XIIIa substrate peptides TG-MMP-Lys and TG-Gln were added to eight-arm PEG vinylsulphone (PEG-VS) in a 1.2-fold molar excess over VS groups in 0.3 M triethanolamine (pH 8.0) at 37 °C for 2 h. The reaction solution was subsequently dialysed (Slide-A-Lyzer 7K, MWCO: 7; or Snake Skin, MWCO 10K, PIERCE) against ultrapure water for 3 days at 4 °C. After dialysis, the product (8-PEG–MMP-Lys and 8-PEG-Gln, respectively) was lyophilized to obtain a white powder.

Factor XIII activation. Activation of factor XIII (FXIII) was achieved as described previously[18]. Briefly, 1 ml of 200 U ml^{-1} FXIII (CSL Behring) was incubated for 30 min at 37 °C with 100 µl of 20 U ml^{-1} thrombin (Sigma-Aldrich) in the presence of 2.5 mM $CaCl_2$. Activated FXIII was aliquoted and stored at −80 °C until use.

Characterization of hydrogel mechanical properties. For convenience, we reproduce below methodological details originally available in ref. 19. Hydrogel discs (30 µl) were made and allowed to swell in 50 mM TBS for 24 h at room temperature. Swollen hydrogel disks of 1 mm thickness were placed between the two plates of a Bohlin CV 120 rheometer (Bohlin Instruments) and compressed up to 80% of their original thickness. Measurements were conducted in constant strain (5%) mode. Shear stress was recorded over the frequency range of 0.1–1 Hz and average storage moduli (G') over the frequency range were obtained. Storage modulus (G') was plotted as a function of PEG content (w/v) for each of the two MMP sensitivities.

Gel functionalization of cell–cell interaction proteins. For convenience, we reproduce below methodological details originally available in ref. 19. The Fc-tag–Protein A conjugation strategy was employed to bind cell–cell interaction proteins to the hydrogel network. The modification of Protein A was achieved by functionalization with a maleimide group by reacting with NHS–PEG–maleimide in 10 molar excess, followed by Gln-peptide attachment through its cysteine side chain. Fc-tagged E-cadherin and EpCAM, (R&D Systems) were premixed with Gln–Protein A in 1.66 molar excess ratios for 30 min at room temperature. The obtained products were aliquoted and stored at −20 °C until use.

3DiPSCs culture and differentiation. Stably reprogrammed 3DiPSCs were collected from hydrogels by TrypLE Express treatment for 10 min at 37 °C and grown for at least three passages on feeder cells in mouse ESC medium. Following this initial step 3DiPSCs can be grown in feeder-free condition in mouse ESCs medium. To differentiate 3DiPSC differentiation into the three germ layers cells were collected by TrypLe Express treatment and transferred to bacterial culture dishes in mouse ESC medium without LIF. After 3 days, embryoid bodies were plated on 0.2% gelatin-coated tissue culture plates and incubated for another 7 days. The differentiation potential was then assessed by immunostaining analysis of TUBB3, FOXA2 and MHC.

Cell viability assay. Calcein AM and ethidium homodimer-I staining (Life Technologies) was carried out following the manufacturer's instructions, and flow cytometry analysis was carried out with a CyAn ADP Analyzer (Beckman Coulter).

Alamar blue assay and alkaline phosphatase staining. To monitor 3D cell growth in PEG matrices, mouse ESC proliferation was quantified by Alamar blue assay (Invitrogen) according to the manufacturer's instructions. Briefly, in this assay, fresh medium containing 10% Alamar blue solution was added to the gel drops and incubated for 6 h at 37 °C. The supernatant was then collected and analysed by Tecan Safire 2 plate reader. The assay was performed every other day over 9 days. Alkaline phosphatase staining was performed according to the manufacturer's instructions using the Alkaline Phosphatase Detection Kit (Millipore).

EdU labelling assay. To analyse cell proliferation, a 1 h pulse of EdU was applied to cells at different time points during 2D or 3D reprogramming. The EdU signal was then revealed using the Click-iT EdU imaging Kit (Life Technologies) according to the manufacturer's protocol. Fluorescence was then analysed by imaging or quantified by FACS analysis.

Immunofluorescence staining. Encapsulated/plated cells were washed with phosphate buffered saline (PBS) for 30 min and fixed with 4% paraformaldehyde (PFA) for 30 min at room temperature. Fixed cells were washed three times with PBS and permeabilized in 0.2% Triton X-100 (Sigma-Aldrich) for 30 min at room temperature. Permeabilized cells were then blocked with 2% bovine serum albumin (BSA; Sigma-Aldrich) for 2 h (or 30 min for 2D cultures) at room temperature. Cells were stained overnight with primary antibody at 4 °C. After three PBS washes, cells were stained with corresponding secondary antibody (1:500; Invitrogen) overnight at 4 °C in the dark (or 1 h at room temperature for 2D cultures). Cells were washed three times with PBS and incubated for 30 min in 4′,6-diamidino-2-phenylindole (Invitrogen) for nuclei visualization. Confocal imaging was carried out using LSM 700 (Zeiss). Images represent the *z*-stack projection of confocal sections. The following antibodies were used: rabbit anti-NANOG (Abcam ref. no. AB80892, 1:100), rabbit anti-hNANOG (Abcam ref no. 21624, 1:200), rabbit anti-SOX2 (Life Technologies ref. no. 481400, 1:200), goat anti-OCT4 (Abcam ref. no. AB27985, 1:100), goat anti-hSOX17 (R&D ref. no. AF1924, 1:200), mouse anti-SSEA-4 (Hybridoma Banks ref. no. MC-813-70, 1:50), mouse anti-SMA (Abcam ref. no. 7817, 1:200), rabbit anti-E-cadherin (Cell Signaling, 1:200), mouse anti-TUBB3 (Covance ref. no. MMS-435P, 1:500), mouse anti-MHC (Hybridoma Bank ref. no. MF-20, 1:50), rabbit anti-FOXA2 (Millipore ref. no. AB4125, 1:200), rabbit anti-acetyl-Histone H3 (Millipore ref. no. 06-599, 1:100), and rabbit anti-H3K4 tri-methylation (Abcam ref. no. AB8580, 1:100).

Flow cytometry. 3DiPSCs were collected from hydrogels by dissociation with TrypLE Express for 20 min at 37 °C. Flow cytometry analysis was carried out with a CyAn ADP Analyzer or Gallios (Beckman Coulter).

Image analysis. For quantification of AcH3 and H3K4me3 fluorescence intensity, ×63 images were processed using algorithms developed in ImageJ software. Briefly, the macro applies the threshold algorithm on the DAPI channel to create a mask (a binary image), detects the particles (using a specified threshold for size) on this mask and measures the mean intensity of the particles (on the channel selected for measurement). E-cadherin+ colony and YAP1+ cell nucleus counting was performed on ten ×63 images from three replicates for each condition.

Western blot. For convenience, we reproduce below methodological details originally available in ref. 45. Three days after 2D or 3D culture 1×10^6 plated fibroblasts were lysed on ice in 50 mM Tris HCl, pH 7.4, 150 mM NaCl, 1 mM EDTA, 1% Triton X-100 with 1× protease cocktail inhibitor (Roche) for 30 min. The protein content of each sample was determined with the Bio-Rad assay kit (Bio-Rad). About 50 g per lane of proteins was separated on 4–20% gradient SDS–polyacrylamide gel (Bio-Rad). Proteins were transferred to nitrocellulose filters (Bio-Rad) in transfer buffer (25 mmol l^{-1} Trizma 193 mmol l^{-1} glycine, 20% methanol, Sigma). Filters were soaked for 30 min in transfer buffer and were

blotted for 2 h in TTBS (10 mmol l^{-1} Tris–HCl pH 8, 150 mmol l^{-1} NaCl, 5%, Tween-20 0.1%, non-fat dry milk, Bio-Rad). Membranes were probed with primary antibodies in TTBS overnight at 4 °C. After washing 4 times for 5 min immunoblots were incubated with HRP-conjugated secondary antibodies in TTBS for 2 h at 25 °C. Western blots were carried out using the ECL method according to the manufacturer's protocol (Amersham Biosciences). The following primary antibodies were used: rabbit anti-acetyl-Histone H3 (Millipore ref. no. 06-599, 1:100), rabbit anti-H3K4 tri-methylation (Abcam ref. no. AB8580, 1:100), rabbit anti-Histone H3 (Millipore ref. no. 06-755, 1:1,000), mouse anti-beta actin (Sigma ref. no. A5441, 1:5,000).

PCR with reverse transcription. Mouse ESCs were collected from hydrogels by dissociation with TrypLE Express for 20 min at 37 °C; RNA extraction was performed using TriPure Isolation Reagent (Roche) according to the manufacturer's instructions. cDNA was synthesized from 1 μg RNA using iScript Select cDNA Synthesis Kit (Bio-Rad), and PCR was carried out with primer sets listed below, using JumpStart Taq DNA Polymerase with UNO Thermal Cycler (VWR). Real-time quantitative RT–PCR was carried out with the primer sets listed below, using iQ SYBR Green Supermix (Bio-Rad) with the Applied Biosystems 7900HT System. The expression of genes of interest was normalized to that of glyceraldehyde 3-phosphate dehydrogenase (*Gapdh*) in all samples. The primers used for PCR amplification are listed in Supplementary Table 2.

Bisulphite sequencing. For the methylation analysis of *Oct4* and *Nanog* promoters by bisulphite sequencing, genomic DNA (gDNA) was extracted using TriPure Isolation Reagent (Roche) and then treated with Epitect Bisulfite Kit (Qiagen) according to the manufacturer's instructions. Converted gDNA were used as templates to amplify target of interest. The resulting PCR products were cloned and sequenced. The primers used for PCR amplification are listed in Supplementary Table 2.

Microgroove substrates, Matrigel and collagen gels. Microgrooves were produced as previously described[15]. 3D Matrigel cultures were obtained by mixing Matrigel and cell suspension at a 1:1 ratio and then incubating the solution for 30 min at 37 °C. 3D collagen I gels were obtained by mixing cell suspension with 0.5% bovine dermis acid-solubilized type I collagen (Koken). Then, 0.4% collagen I gels were obtained by neutralizing the pH according to the manufacturer's instructions. The amount of cells and the 3D reprogramming protocol used for Matrigel and collagen I gels was the same as indicated for the PEG hydrogels.

Teratoma formation assay. Immunodeficient NSG mice (NOD.Cg-*Prkdc*^{scid} *Il2rg*^{tm1Wjl}/SzJ) were used for the teratoma formation assay. Five mice were injected subcutaneously with 1×10^6 cells (200 μl volume, 50% Matrigel) of mouse or human 3DiPSCs. Animals were observed twice a week for tumour growth. Tumour size was measured with a calliper and animals were euthanized after 6 weeks or after development of tumours larger than 1 cm^3. Tumours were then dissected out and subjected to haematoxylin and eosin staining.

Chimaeric mice generation. Chimaeric mice were generated by the EPFL Transgenic Core facilities (http://tcf.epfl.ch/site/tcf/page-6759.html). For convenience, we reproduce below methodological details originally available in ref. 46. Blastocysts were collected from the oviduct of superovulated CD-1 females mated with CD-1 males 48 h earlier by a flushing procedure with ESC medium. The zona pellucida was removed from the embryos by washing through 3 consecutive drops of Acid Tyrode solution (Sigma). Single cells were generated after treatment with trypsin. Between 5 and 15 3DiPSCs were injected in each embryo and cultured in ESC Knockout replacement serum medium overnight at 37 °C 5% in 5% CO_2. The following day, blastocysts were transferred into the uterus of pseudopregnant recipient CD-1 females mated with vasectomized CD-1 males 2.5 days earlier.

HTS robotic mixing and dispensing. For convenience, we reproduce below methodological details originally available in ref. 19. High-throughput combinatorial screening of 3D microenvironments was performed as described using a Hamilton Microlab StarPlus automatic liquid handling robot with a Nanopipettor head. All automated steps were programmed with MicroLab Vector Software version 4.1.1 (HAMILTON Bonaduz AG). In brief, 8 combinations of PEG precursor solutions (comprising 2 MMP sensitivities ×4 stiffnesses; MMP sensitivities were controlled by incorporating the two MMP substrates GPQG↓IWGQ and VPMS↓MRGG in the gel backbone) were mixed robotically and aliquoted into wells of a 384-well plate. ECM proteins and peptides were thawed on ice and dispensed (including blank control) into the gel precursor-filled wells to produce hydrogel precursors with 64 unique combinations of mechanical properties (MP), MMP sensitivities/degradability (DG) and ECM components (EC). A 96-well plate was prepared with differentiation medium containing the soluble factor CHIR99021 (3 μM) and a blank control.

Fibroblasts were trypsinized and resuspended at a concentration of 2×10^6 cells ml^{-1} and kept on ice. Simultaneously, frozen aliquots of FXIIIa were thawed and also kept on ice. Cells were then dispensed into the wells containing gel precursors, followed by dispensing and mixing of FXIIIa. The final volume of each gel was 4 μl. These cell-containing hydrogel mixtures were then immediately dispensed into a 384-well plate, incubated for 20 min, followed by having media containing CHIR or a blank control dispensed in a timed, automated manner.

High-throughput imaging. For convenience, we reproduce below methodological details originally available in ref. 19. Plates were fixed with 4% paraformaldehyde 8 days after induction of reprogramming and then stained with DAPI. Imaging was performed on a BD Pathway 435 automated imaging system (BD Biosciences). At every *xy*-position, that is, for every well, 6 images were captured across a *z*-stack height of 800 μm. For each well, these 6 images in each channel were collapsed into a single additive image.

All images were processed using algorithms developed in CellProfiler v.9777 (Broad Institute). Collapsed image stacks for each well in the GFP, DAPI channels were input. In an initial analysis, DAPI images were subjected to a threshold and segmented to obtain total colony numbers per well. This DAPI-based segmentation was then used as a mask for the GFP images. The GFP intensity across all colonies was analysed and correlated with corresponding images, and a threshold determining GFP-positive colonies was identified. In a second analysis, GFP images were subjected to a threshold with the stringent criterion identified in the first analysis to determine the number of GFP-positive colonies in each well. Morphometric and GFP intensities were also identified in this second analysis.

HTS data processing and statistical analysis. For convenience, we reproduce below methodological details originally available in ref. 19. Matlab R2010b (Mathworks) was used to process and visually explore the data. Data for each well were averaged over experimental triplicates to obtain averages, standard deviations and standard errors of the mean for each unique microenvironmental condition. The 'number of GFP-positive colonies (count per well)' output was selected from this data set and ranked. The top 20% of all conditions (26 conditions out of 128) were extracted from this ranked set and their corresponding microenvironmental conditions were identified. Each microenvironment in these top conditions was represented by a set of 4 numbers corresponding to a category (MP, DG, EC, SF). For the identified 26 top conditions, counts for each condition within each category were added, and all counts were represented as a percentage within each category.

To perform hierarchical clustering on the entire data set, all measurements in wells where no colonies were identified were set to 0. The data were then centred to have a mean of 0 and scaled to have a standard deviation of 1. Hierarchical clustering with a Euclidean distance metric and average linkage was performed to generate the hierarchical tree. Conditions identified for each cluster were then represented as for the ranked values above.

To construct the generalized linear models, data were first input into R V2.14.2. GLM models, which took into account all possible interaction terms specified for analysis of number of GFP-positive colonies. The step AIC procedure was run to obtain optimal models based on the Akaike criterion. The GLM procedure in SAS v9.0 software (SAS Institute) was used to compute a least-squares mean value for each factor within every category, and differences of least-squares means ± standard errors with the control were tested for significance. The used models considered the effects of MP, DG, EC and SF, as well as interactions determined to be significant. For all parametric tests, normality of the residues and homogeneity of the variance were examined in QQ and Tukey–Anscombe plots, respectively.

Human 3D iPSCs. Human neonatal foreskin fibroblasts (1.5×10^5; ATCC) were infected twice at 24 h intervals, with a lentiviral vector-expressing human *OCT4*, *SOX2*, *KLF4* and *MYC* (OSKM) driven by a SFFV promoter. Successively, infected cells were collected and either replated on mitomycin-inactivated mouse embryonic fibroblasts (2D standard condition) or encapsulated in PEG hydrogels (3D standard or HTS conditions). The following day, the medium was replaced by mTeSR-1 (Stemcell Technologies) and thereafter changed daily. After 6 weeks, PEG hydrogels with human 3DiPSCs were digested with TrypLE Express, and cells were replated plated on a 6-well plate, coated with hESC-Matrigel (Corning). Human 3DiPSCs were grown in mTeSR-1 and passaged in 1:5 ratio using ReLeSR (Stemcell Technologies). Multilineage differentiation was performed by plating human 3DiPSCs as single cells on Matrigel and inducing for 30 days meso-endodermal or neural fate respectively with fibroblast medium or DMEM/F12/B27. The differentiation into the three germ layers was assessed by immunostaining analysis for TUBB3 (neuroectoderm), SMA (mesoderm) and SOX17 (endoderm).

Lentivirus preparation. HEK 293T cells were cultured in DMEM, supplied with 10% FBS, 10 U ml^{-1} penicillin, streptomycin 10 μg ml^{-1}, 2 mM glutamine, 1 mM sodium pyruvate and 100× non-essential amino acids. For the transfection, 7.5×10^6 HEK 293T cells were seeded on 15 cm dishes and incubated overnight. The following mix was prepared for the transfection: 22 μg of SFFV-OKSM, 7.9 μg of VSV-G and 14.6 μg of Gag-Pol-Rev-Tat in 1.125 ml of water. Successively, 125 μl of $CaCl_2$ 2.5 M and 1.25 ml of HBS were added to the mix while vortexing at full speed. The final mix was then dropped over the cells. After 48 h the supernatant

was collected and ultracentrifuged at 50,000*g* for 2 h at 20 °C. The pellet with viruses was resuspended in PBS and stored at −80 °C.

Statistical analysis. Data were analysed by using the paired/unpaired Student's *t*-test or, in case of more than 2 experimental groups, by one-way analysis of variance (ANOVA) followed by *post hoc* Bonferroni's multiple comparison test using GraphPad Prism 6.0 statistical software (GraphPad Software). Significance level was preset to $p < 0.05$. Data are expressed as means ± s.e.m., with *n* denoting the number of samples analysed. All represented experiments were performed at least three times.

References

45. Volpicelli, F. *et al.* Bdnf gene is a downstream target of Nurr1 transcription factor in rat midbrain neurons *in vitro*. *J. Neurochem.* **102,** 441–453 (2007).
46. Di Stefano, B. *et al.* An ES-like pluripotent state in FGF-dependent murine iPS cells. *PLoS ONE* **5,** e16092 (2010).